J. Fluid Mech. (1974), *vol.* 63, *part* 4, *pp.* 773–800
Printed in Great Britain

On the interaction of internal waves and surface gravity waves

By JOHN E. LEWIS,† BRUCE M. LAKE AND DENNY R. S. KO‡
Fluid Mechanics Laboratory, TRW Systems, Redondo Beach, California

(Received 3 May 1973 and in revised form 12 November 1973)

The perturbation of pre-existing surface gravity waves caused by the presence of an internal wave was studied both experimentally and analytically. An extensive series of experiments was performed, and quantitative results were obtained for the one-dimensional monochromatic interaction of internal waves and surface gravity waves. Internal wave-induced surface slope, amplitude and wavenumber modulations were measured for a wide range of interaction conditions. A complementary theoretical analysis, based on the conservation approach of Whitham (1962) and Longuet-Higgins & Stewart (1960, 1961), was performed and a closed form solution obtained for the one-dimensional wave interaction. Both the theory and the experiment demonstrate that the effect increases with interaction distance. The maximum interaction effect is found to occur when the phase speed of the internal wave and the group velocity of the surface wave are matched. The phase of the internal wave at which maximum surface-wave modulation occurs is found to be a sensitive and continuous function of the relative wave speeds. The experimental data are in good agreement with the present theoretical analysis.

1. Introduction

The perturbation to oceanic surface waves caused by the presence of an internal wave has been a subject of oceanographic interest for many years. The observations by Ewing (1950), LaFond (1962) and Gargett & Hughes (1972) in coastal waters have presented ample evidence for the existence of this interaction. Previous studies have not, however, led to quantitative conclusions. To isolate, identify and control the influence of physical parameters on the interaction, we examined an idealized internal-wave/surface-wave system in the laboratory. The interaction of a linear, one-dimensional monochromatic surface gravity wave train with an independently generated monochromatic internal-wave train, propagating in the same direction, was studied in a two-fluid tank. Measurements of surface-wave amplitude and slope and internal-wave amplitude were used to determine quantitatively interaction-induced surface slope,

† Present address: Techmate, Inc., Torrance, California.
‡ Present address: Flow Research, Inc., Los Angeles, California.

amplitude and wavenumber modulations, and their dependence on relative wave speed, interaction distance and internal-wave characteristics.

Theoretical investigations using the radiation stress concepts derived by Longuet-Higgins & Stewart (1960, 1961) have also been reported by various authors (e.g. Gargett & Hughes; Phillips 1971). However, these studies were based on a steady-state analysis, which assumes the interaction phenomenon to be time-independent in a frame moving with the internal-wave phase speed. The non-steady interaction problem was first addressed analytically by Hartle & Zachariasen (1968). Using transform techniques on the linearized governing equations, the modulation of the surface waves caused by the presence of an internal-wave field was shown to increase with time or interaction distance. To provide insight into this type of interaction, we studied an idealized internal-wave/surface-wave system analytically, to complement the detailed laboratory experiments. The analytical approach follows the theories of Longuet-Higgins & Stewart, and Whitham (1962), which have been successfully applied to steady-state problems.

2. Experiment

2.1. *Apparatus*

Figure 1 shows a schematic, illustrating the laboratory experiment. A simple two-fluid system, consisting of a layer of water lying above a heavier fluid, was used to establish the internal gravity waves, with both surface and internal waves generated at an initial station, $x = 0$. The experiment was performed in a $3 \times 3 \times 40$ ft tank, designed to generate independently both surface waves and internal gravity waves. The tank was filled with pure water over a 3 in. depth of a denser mixture of freon and kerosene. Wave makers were located at one end of the tank to generate surface and internal waves, and shallow angle wave absorbers were installed at the opposite end to attenuate wave reflexions. A carriage, which was rail-mounted over the tank and could be moved to any location along the full tank length, was used as an instrumentation platform. To keep the working fluids in the facility clean, and to ensure that the dynamics of the surface waves are not subject to effects of surface films, the facility was provided with two 5μ filtering systems, including a surface skimmer and an ultra-violet sterilizer for the distilled water. The skimmer and plumbing inlets were removed and the filter systems shut down during experiments, so that these systems in no way interfered with fluid motions during wave interaction measurements.

The wave-generating mechanisms are shown schematically in figure 2. Internal waves were generated by means of a piston moving in a channel, as shown in the figure. Since the interaction distance is an important wave interaction parameter, the system was designed to create as 'clean' an internal wave as possible from the initial station. For shallow interfacial waves the lower velocity field was nearly constant, and was well approximated at $x = 0$ by the piston motion in the constant area channel. For the ideal case, the volume fluxes above and below the interface are equal and opposite. This overall conservation was satisfied by

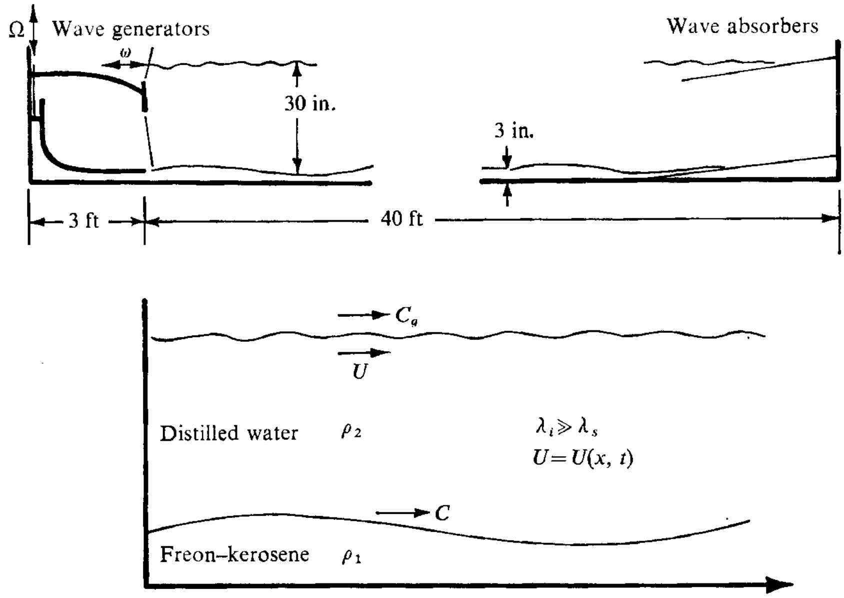

Figure 1. Schematic representation of wave interaction experiment.

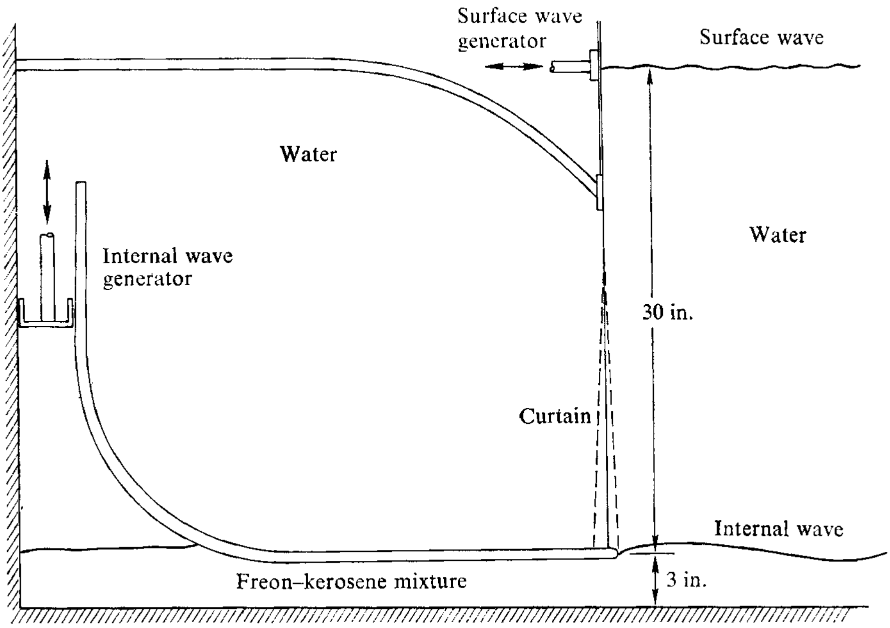

Figure 2. Schematic diagram of wave generators.

enclosing the upper surface of the internal-wave maker as shown in figure 2. The velocity distribution in the upper fluid was approximated by a rigid flap, also shown in figure 2, hinged 18 in. above the interface.

The phase velocity and wavelength of the internal wave could be varied independently. This was accomplished by simultaneously varying the specific

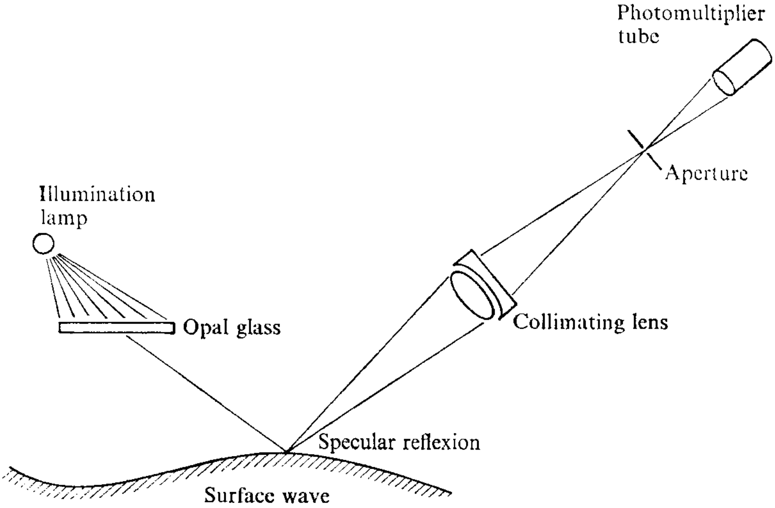

FIGURE 3. Schematic diagram of wave slope measuring device.

gravity of the freon–kerosene mixture and the frequency of the internal-wave generation (using a variable speed motor). Surface waves were generated by a rigid flap hinged 3 in. below the air–water surface. The frequency, and hence the propagation velocity, of the surface waves could be varied independently of the internal-wave characteristics.

The structure that supported the wave-generating motors was isolated from the tank. Mechanical contact between the wave generators and the tank was also carefully avoided. At the opposite end of the tank were shallow angle wave absorbers. A simple impermeable wave absorber was used for surface waves, and was very effective ($A_{\text{reflected}}/A_{\text{incident}} \leqslant 5\,\%$, where A is the wave amplitude). An impermeable absorber surface with a 3 in. depth of porous brass pads was used to reduce internal-wave reflexions to levels ($A_{\text{reflected}}/A_{\text{incident}} \leqslant 7\,\%$) acceptable for experimentation under steady-state operating conditions in the facility.

The data presented here are measurements obtained from two resistance wave-amplitude gauges, one for the internal wave and one for the surface wave, and an optical device developed to measure the surface-wave slope directly. The following summarizes the important characteristics of these instruments. The operation and calibration of the instruments is described in detail, including calibration data, in Lewis & Lake (1973).

The device developed for the slope measurement is shown schematically in figure 3. The basic principle is quite simple, and relies on specular reflexion from the local water surface. A lens system focuses on a spot 1 mm × 1 cm (the smaller dimension is in the direction of wave propagation), and feeds into a photomultiplier tube light whose intensity depends on the slope of the surface. Detailed calibrations were performed, which showed that the device has linear response to surface slope over a range of $\pm 14°$.

Although 'in place' calibration checks could be performed with the slope gauge mounted on the wave tank instrument carriage (as described in § 2.2), the detailed calibrations were performed with the gauge mounted on a specially designed calibration apparatus. The calibration apparatus was designed to reproduce exactly the carriage-mounted configuration of the gauge with respect to its reflecting surface. Three interchangeable reflecting surface control mechanisms were provided to permit separate calibrations for gauge sensitivity to vertical displacement, slope and curvature. This was accomplished by vertically displacing, inclining or bending reflecting surface plates, to produce accurately controlled displacements, slopes or curvatures, respectively. For slope and curvature calibrations, the point on the reflecting surface at which the optics were focused was at fixed height and, in the case of curvature, at the point of zero surface slope, to ensure that each calibration isolates the specific quantity of interest. Calibrations for gauge response to vertical displacements over a $\pm 0{\cdot}2$ in. range show linear response to displacements with sensitivity corresponding to 1 % in measured slope for the surface waves in these experiments. Calibrations for response to curvature over a $\pm 0{\cdot}1$ in.$^{-1}$ range (wave curvature in these experiments is $0{\cdot}02$–$0{\cdot}3$ in.$^{-1}$) show that the optical gauge has no measurable response to surface curvature. To perform such calibrations, it was necessary to focus the gauge optics on the point of zero slope on the reflecting plate. When the focal point was focused on a point slightly offset from the point of zero slope, the gauge output signal showed an apparent variation with changes in plate curvature. In such a case, accurate measurement of the focal point offset distance from the zero slope point and calculation of the slope of the reflecting plate at the actual focal point showed that such gauge response could always be fully accounted for by sensitivity to slope alone. Furthermore, by locating carefully the focal point at the point of zero slope, it was always possible to perform curvature 'calibrations' in which the gauge output showed no measurable variation while the reflecting surface plate was continuously deformed over the full range of surface curvature. Since gauge output voltage changes of one part in one thousand were easily measurable, the calibration results put an upper bound on possible curvature-induced contributions to the optical gauge output signal of less than 1 % in slope for all surface waves used in the experiments.

Periodic calibrations of the optical gauge, on the calibration device ($\pm 14°$ range†) and on the instrument carriage ($\pm 2{\cdot}5°$ range), demonstrated that the gauge response to slope was always linear. In addition, the calibrations showed that setting the light source intensity so that the zero-slope (d.c.) output voltage level of the photomultiplier tube was maintained constant resulted in a reproducibly constant sensitivity to slope. Constant sensitivity was not a critical requirement, since the primary measured quantity was fractional change in slope, which required only linearity. Because constant sensitivity could be maintained, however, absolute wave slopes, as well as fractional changes in wave slopes, were measured for the entire series of experiments. As used in the

† Detailed calibrations for these experiments were performed over a $\pm 6{\cdot}2°$ range of surface slope. More recent calibrations, using a slightly modified configuration, showed the gauge to have a useful linear range of $\pm 14°$, although linearity over the wider range is not as good as for the $\pm 6{\cdot}2°$ range.

experiments, the gauge had 34·1 mV degree^{-1} sensitivity to slope, with an r.m.s. average deviation of all calibration data points from the least-squares linear fit to the data of only 2·8 mV.

Calibrations of the resistance wave gauges before and after series of measurements showed that, during each series, linearity and sensitivity of the gauges remained constant within the resolution of the calibration data. Over periods of days or weeks, however, sensitivity changes of as much as 10 % might occur as a result of the corrosive effects of the liquids on the wires, and periodic cleaning of the wires with nitric acid to remove corrosion. For this reason, the resistance gauges were recalibrated for each series of experiments. All calibrations were performed with the gauges mounted on the instrumentation carriage and vertical displacements measured to within 0·001 in., as described in § 2.2. The internal gauge sensitivities were typically 6 V in.$^{-1}$ with linearity over a $\pm$ 0·5 in. range. Surface gauge sensitivities were typically 16 V in.$^{-1}$ with linearity over a $\pm$ 0·2 in. range. The typical r.m.s. average deviation of the calibration data points from the least-squares linear fit to each set of calibration data was only 0·04 V for the internal gauge, and 0·06 V for the surface gauge.

2.2. *Procedure*

The experiments were done to study interactions of monochromatic surface and internal waves. Power spectral densities of the individual surface and internal wave conditions used in the experiments were obtained, to assess the extent to which the waves generated in the facility were actually monochromatic. Power spectra, obtained from the tape recordings of the internal resistance gauge for steady operation of the internal wave maker (with no surface waves present), showed that the internal waves used were reasonably monochromatic, with second harmonic energy density less than the primary frequency energy density by at least -16 db in all cases, and more typically by -25 db. The power spectrum of each experimental surface-wave condition (with no internal waves present) was obtained from tape recordings of the outputs of both the surface resistance gauge and the surface-wave slope gauge. The results showed that all surface waves used in the experiments were closely monochromatic, with energy density in second harmonics below energy density in primary frequencies by -23 to -30 db, or more. In these investigations of ambient surface- and internal-wave conditions, the spectra described above were obtained at 5 ft intervals for $x = 5$–30, and at $x = 33$ ft. Examples of these spectra may be found in Lewis & Lake (1973).

The two resistance gauges and the optical wave slope gauge were mounted on the wave-tank instrument carriage, and could therefore be positioned at any location along the tank simply by moving the carriage, leaving their relative positions unaffected. The relative gauge locations on the carriage were set so that all three measurements were made at the same x location in the tank. The two resistance gauges were mounted on the carriage on motor-driven shafts coupled to Selsyn position indicators, so that 'in-place' calibrations could be performed by moving the gauges over a range of vertical positions. The gauges were recalibrated for each set of measurements, the surface gauge over a 0·8 in. range centred about the air–water interface, and the internal gauge over a 1·6 in. range centred about the two-fluid interface, with vertical displacements accurate to better than 0·001 in. given by the position indicators.

The optical slope gauge was mounted on the carriage in such a way that the height of the gauge above the water surface at the location of the focal point of the optical system was fixed. The gauge could be rotated around a horizontal axis perpendicular to the x direction at the same location. It was therefore possible to set the gauge at a range of inclination angles over the undisturbed water surface in a way that was equivalent to the presence of the same range of surface slope angles under the gauge in its fixed operating position. This arrangement was used to perform 'in-place' calibration checks (over a $\pm 2{\cdot}5^\circ$ range) of the detailed gauge calibrations described in § 2.1.

For each set of measurements, internal waves of fixed frequency were continuously generated. Experiments to identify the dependence of wave interactions on relative wave speeds were performed by making measurements at a fixed x location in the tank for a range of surface-wave speeds. Data samples of 2 min were recorded for each surface-wave speed, separated by 2–4 min intervals, during which no surface waves were generated and the upper surface was allowed to return to an undisturbed state. Experiments to identify the dependence of wave interactions on interaction distance were performed by continuously generating surface waves of fixed frequency and making measurements for a range of carriage locations along the tank. Data samples of 2 min were recorded at each station at 1 ft intervals for $x = 5$–33 ft. Series of experiments of each type were performed for two fluid density ratios and internal-wave frequencies, to obtain measurements identifying the dependence of wave interactions on these parameters as well. To ensure that the surface waves were not subjected to effects of surface films, the upper fluid surface was periodically skimmed clean. During all experiments, the output signals of the three gauges and an identifying coded time signal were simultaneously recorded on tape using an Ampex FR 1300 FM tape recorder. The gauge outputs were also visually monitored and recorded using an oscillograph recorder.

The experiments were performed for the following conditions. Surface wave: $2{\cdot}18 \leqslant \omega \leqslant 4{\cdot}45$ c/s, $0{\cdot}29 \leqslant \lambda_s \leqslant 1{\cdot}10$ ft. Internal wave: $0{\cdot}21 \leqslant \Omega \leqslant 0{\cdot}26$ c/s, $3{\cdot}2 \leqslant \lambda_i \leqslant 4{\cdot}4$ ft. Fluid density ratio $= 1{\cdot}152$, $1{\cdot}288$. Measurement station along tank: $x = 5$–33 ft at 1 ft intervals (ω and Ω are wave frequency and λ is the wavelength). Surface-wave amplitudes and slopes were of order 0·05 in. and 2–6°, respectively. Internal-wave amplitudes were 0·15–0·30 in., depending on the internal-wave conditions used and location along the tank (as described in § 2.3). The ranges of the basic dimensionless parameters were therefore $0{\cdot}75 < C/C_{g0} \leqslant 1{\cdot}4$, $5 \leqslant Kx \leqslant 60$, $4 \times 10^{-4} \leqslant u_0/C \leqslant 10^{-3}$, $0{\cdot}07 \leqslant \lambda_s/\lambda_i \leqslant 0{\cdot}31$. ($C$ is the phase velocity of the internal wave, C_{g0} is the group velocity of the undisturbed surface wave, K is the wavenumber of the internal wave and u_0 is the surface velocity induced by the internal wave.) The experiments were performed for the combinations of these conditions shown in table 1.

Cases	Density ratio ρ	Ω (c/s)	ω (cps)	x (ft)	Total runs†
Modulations against interaction distance	1·152	0·256	3·28	$\left\{\begin{matrix} x = 5, 6, 7, \ldots, 33 \\ 28 \text{ values} \end{matrix}\right\}$	84
$\left(\begin{matrix} \text{'Resonant' interactions} \\ C/C_{g0} \simeq 1 \end{matrix}\right)$	1·152	0·204	2·97	$\left\{\begin{matrix} x = 5, 6, 7, \ldots, 33 \\ 28 \text{ values} \end{matrix}\right\}$	84
	1·288	0·263	2·28	$\left\{\begin{matrix} x = 5, 6, 7, \ldots, 33 \\ 28 \text{ values} \end{matrix}\right\}$	84
Modulations against relative wave speed	1·152	0·256	$\left\{\begin{matrix} 2{\cdot}18 \leqslant \omega \leqslant 4{\cdot}45 \\ 41 \text{ values} \end{matrix}\right\}$	30·0	123
$\left(\begin{matrix} \text{1st case: maximum } Kx = 58 \\ \text{2nd, 3rd and 4th: matched} \\ Kx \simeq 43 \end{matrix}\right)$	1·152	0·263	$\left\{\begin{matrix} 2{\cdot}18 \leqslant \omega \leqslant 4{\cdot}45 \\ 41 \text{ values} \end{matrix}\right\}$	22·2	123
	1·152	0·208	$\left\{\begin{matrix} 2{\cdot}18 \leqslant \omega \leqslant 4{\cdot}45 \\ 41 \text{ values} \end{matrix}\right\}$	28·97	123
	1·288	0·260	$\left\{\begin{matrix} 2{\cdot}18 \leqslant \omega \leqslant 4{\cdot}45 \\ 41 \text{ values} \end{matrix}\right\}$	30·85	123

† Each interaction condition independently reproduced and remeasured three times during experimental study.

TABLE 1. Matrix of monochromatic wave interaction experiments

2.3. *Data reduction*

In general, the data were reduced by replaying tape-recorded gauge outputs through analog processing equipment into a high-speed digital voltmeter and printer. At the same time, the recorded time-code signals were passed through a time-code reader into the printer. Two columns of printer output were produced at twenty samples per second, one giving the value of the measured quantity of interest, the other the appropriate identifying time code.

The internal-wave-induced fractional changes in surface-wave amplitude

$$A^* = \frac{A_{\max} - A_{\min}}{A_{\max} + A_{\min}} \quad \text{and slope} \quad m^* = \frac{m_{\max} - m_{\min}}{m_{\max} + m_{\min}}$$

were obtained by replaying the recorded surface gauge output signals (at four times recording speed) through an r.m.s. meter into the voltmeter–printer system. The resultant voltage time histories were linearly related to the time history (periodic with the internal-wave period) of the magnitude of the envelope of the surface-wave amplitude and slope modulations. The maxima and minima obtained from these records over a 1 min (recording time) segment of each data sample were used to calculate an average value of the fractional change in amplitude and slope for each data sample.† Each measured value of A^* and m^* is therefore an average, over 12–15 internal-wave periods, of the surface-wave modulation produced by the interaction of surface and internal waves for each

† Absolute amplitudes and slopes were calculated from typical r.m.s. voltage histories covering the range of experimental conditions, using the appropriate tape recorder, r.m.s. meter and wave gauge calibration constants.

set of experimental conditions. The r.m.s. deviation of the individual values from each calculated average was typically 2–10 %.

Surface- and internal-wave frequencies were obtained by replaying the recorded gauge output signals (at eight times recording speed and thirty-two times recording speed, respectively) through a sensitive (62·5 mV cycle^{-1}), linear frequency-to-voltage converter into the voltmeter–printer system. The resultant voltage time histories show that the internal-wave frequency was constant during each data sample period. This was also true of the surface-wave frequency, except that, for strong interactions, the data show sinusoidal modulations with amplitudes equal to several per cent of the mean level, and periods equal to the internal-wave periods. The mean value of the frequency was taken as the ambient surface-wave frequency for these cases. In addition, the modulation data were used to calculate average values of

$$\omega^* = \frac{\omega_{\max} - \omega_{\min}}{\omega_{\max} + \omega_{\min}},$$

the fractional change in surface-wave frequency induced by wave interactions, in the same way that average values of A^* and m^* were calculated. The fractional change in surface wavenumber was then calculated from ω^* using the relation

$$k^* = \frac{k_{\max} - k_{\min}}{k_{\max} + k_{\min}} = 2\omega^* - \frac{u_0}{C_{g0}},$$

where the second term accounts for the surface-current-induced Doppler contribution to the measured value of ω^*.

The group velocity and wavelength of the surface waves were calculated using the measured frequency. The surface current, phase velocity and wavelength of the internal wave were calculated, using the measured frequency, density ratio and amplitude and the formulae given by Neumann & Pierson (1966). For each data sample, the internal-wave amplitude was obtained by averaging the internal resistance gauge measurements over the same sample period used to average A^* and m^*. In addition, because dissipative effects produced a variation in internal-wave amplitude along the tank (and therefore a variation in the magnitude of the surface current), the surface current was evaluated for each set of experimental conditions, using the average amplitude between $x = 0$ and the x location of the measurement station. The rate of amplitude decay for each internal-wave condition was obtained from the measurements of internal-wave amplitude at each x location along the tank. The average upstream amplitude was then calculated for each data sample, using the amplitude at the measurement station during that data sample and the appropriate internal-wave amplitude decay rate. For the internal waves used in these experiments, the amplitude variation down the tank was well approximated by linear decay with rates of 2–5 × 10^{-3} in. per ft of tank length (as shown in Lewis & Lake 1973).

The phase of the internal wave at which the maximum surface-wave modulation occurs has also been determined for the range of relative wave speeds. These results were obtained from expanded-scale oscillograph records of the tape-recorded gauge output signals. In this way, the internal-wave phase location of the maximum surface-wave modulation could be determined to within approximately $\pm 10°$.

An oscillograph record (with horizontal scale compressed to show many internal-wave periods) of the gauge output signals for a nearly resonant ($C/C_{g0} \simeq 1$) wave interaction is shown in figure 4 (plate 1). The figure shows a time history of measurements before and after arrival of an internal wave at the measurement station, to allow one to compare surface-wave conditions with and without internal-wave interactions. It is easily seen that the originally sinusoidal surface wave became modulated in time, at a frequency corresponding to that of the internal wave. Some of the surface waves were enhanced in amplitude and slope, others were depressed. Also shown is the output of a frequency-to-voltage converter operating on the surface-wave gauge signal, which shows the onset of surface-wave frequency modulations at the internal-wave frequency. These experimental data were used to identify the dependence of these effects on physical parameters, such as interaction distance Kx and the ratio of wave speeds C/C_{g0}.

3. Theory

3.1. *General governing equations*

Let the surface current field caused by the internal wave be denoted by $U(\bar{x}, t)$, and let it be a slowly varying function in both x and t. The kinematic wave conservation equation is given by

$$\partial\bar{k}/\partial t + \nabla\omega = 0, \tag{3.1}$$

where $\bar{k}(\bar{x}, t)$ denotes the surface wavenumber, and ω the corresponding frequency. For a deep surface-wave train in the presence of a current field, the dispersion relation is given by

$$\omega = (gk)^{\frac{1}{2}} + \bar{k}\,.\,\bar{U}. \tag{3.2}$$

Here k denotes the magnitude of $\bar{k}$ and g the gravitational acceleration. The second term in (3.2) is a Doppler effect resulting from the surface current. Substitution of (3.2) into (3.1) yields

$$\partial\mathbf{k}/\partial t + (\mathbf{C}_g + \mathbf{U})\,.\,\nabla\mathbf{k} = -\mathbf{k}\,.\,\nabla\mathbf{U}, \tag{3.3}$$

where

$$\mathbf{C}_g = \tfrac{1}{2}(g/k)^{\frac{1}{2}}\hat{\mathbf{k}}, \tag{3.3a}$$

denotes the group velocity of the surface wave when the surface current is absent and $\hat{\mathbf{k}}$ is the unit k vector. For a given current field $\mathbf{U}$, (3.3) can be solved to obtain the wavenumber variation of the surface-wave train.

To obtain information about the wave amplitude, the concept of radiation stress, as introduced by Longuet-Higgins & Stewart (1960, 1961), has been used. The energy equation for an inviscid wave train can be written as

$$\partial E/\partial t + \nabla\,.\,[(\mathbf{U} + \mathbf{C}_g)\,E] = -\mathbf{S}\,.\,\nabla\,.\,\mathbf{U}, \tag{3.4}$$

where E is the energy density of the surface wave. In the case of deep-water surface waves, the radiation stress tensor $\mathbf{S}$ is given by

$$\mathbf{S} = \begin{pmatrix} \frac{1}{2}E & 0 \\ 0 & 0 \end{pmatrix}, \tag{3.5}$$

i.e. the only non-vanishing component of the radiation stress tensor is in the direction of the wave train, and equal to $\frac{1}{2}E$ (see e.g. Phillips 1969). As interpreted by Whitham (1962), (3.4) merely states the conservation of wave energy. In the case of a small-amplitude surface wave, the energy density E is proportional to the square of the wave amplitude A. Hence, the energy conservation equation can be written

$$\partial A^2/\partial t + \nabla . [(\mathbf{U} + \mathbf{C}_g) A^2] = -\tfrac{1}{2}A^2\hat{\mathbf{k}}.\nabla(\mathbf{U}.\hat{\mathbf{k}}). \tag{3.6}$$

Because of the dependence of $\mathbf{C}_g$ on the wavenumber $\mathbf{k}$, (3.6) must be solved after the solutions to (3.3) are obtained.

A general solution to the complete set of small-amplitude equations is not attempted here. Instead, the study has been directed toward the one-dimensional wave interaction corresponding to the laboratory conditions.

3.2. *One-dimensional waves*

Figure 5 shows schematically the configuration to be studied, which corresponds closely to the laboratory experiment. The surface-current field is generated by the interfacial waves of a two-fluid system with frequency Ω and phase speed C for $t > 0$. An independent surface-wave generator with frequency ω is used to produce for all time a single surface-wave train with wavenumber k_0 and unperturbed group velocity C_{g0}. The problem is to determine the change in the surface-wave characteristics as functions of both position x and time t, when the internal-wave-induced surface-current field is present.

For these one-dimensional waves, the governing equations are further simplified. The wave conservation equation (3.3) becomes

$$\frac{\partial k}{\partial t} + (C_g + U)\frac{\partial k}{\partial x} = -k\frac{\partial U}{\partial x}, \tag{3.7}$$

with $\quad C_g = \frac{1}{2}(g/k)^{\frac{1}{2}} \quad \text{and} \quad U = U(x,t).$

The energy conservation equation (3.6) reduces to

$$\frac{\partial A^2}{\partial t} + \frac{\partial}{\partial x}[(C_g + U)A^2] = -\tfrac{1}{2}A^2\frac{\partial U}{\partial x}, \tag{3.8}$$

which can be written in the alternative form

$$\frac{\partial A^2}{\partial t} + (C_g + U)\frac{\partial A^2}{\partial x} = -\tfrac{3}{2}A^2\frac{\partial U}{\partial x} - A^2\frac{\partial C_g}{\partial x}. \tag{3.9}$$

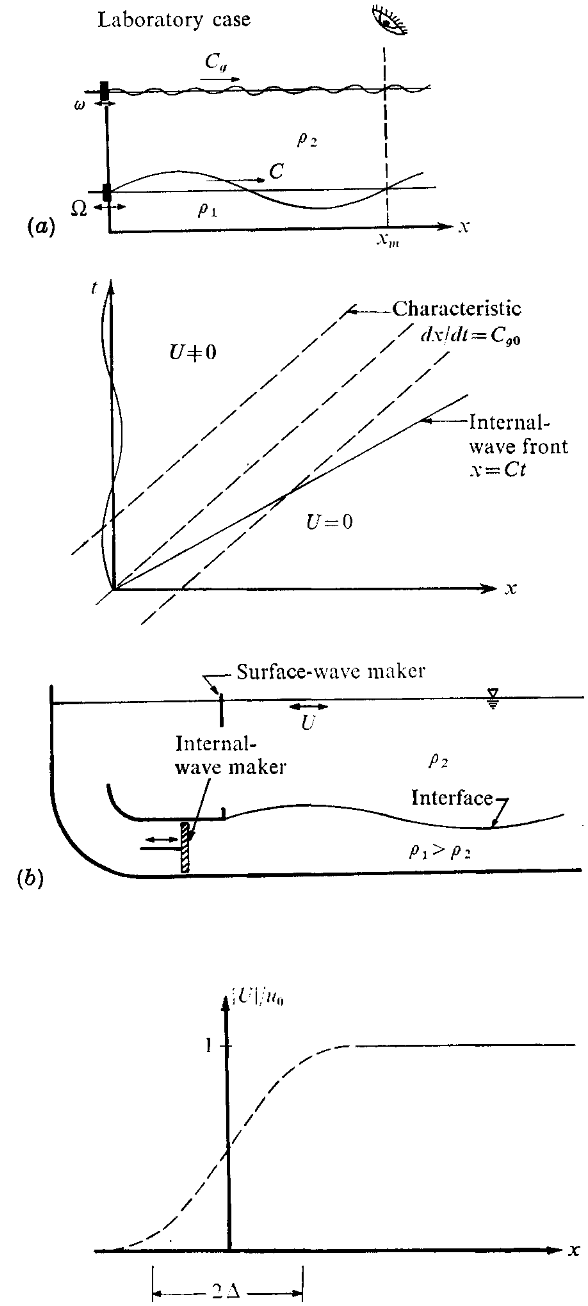

FIGURE 5. (a) Schematic problem definition for laboratory experiment. (b) Schematic diagram of wave tank and estimate of surface current amplitude near wave makers.

Both (3.7) and (3.8) are written in a characteristic form for which the solution can be readily obtained. These characteristics are defined by

$$\frac{dx}{dt} = C_g + U, \tag{3.10}$$

along which the two governing equations reduce to

$$\frac{dk}{dt} = -k\frac{\partial U}{\partial x} \tag{3.11}$$

and

$$\frac{dA^2}{dt} = -\tfrac{3}{2}A^2\frac{\partial U}{\partial x} - A^2\frac{\partial C_g}{\partial x}. \tag{3.12}$$

In other words, in the characteristic co-ordinate system defined by integrating (3.10) such that

$$x = x(\tau, \xi), \quad t = \tau, \tag{3.13}$$

where ξ = constant denotes a characteristic, the governing equations (3.11) and (3.12) become

$$\left.\frac{\partial \ln k}{\partial \tau}\right|_{\xi} = -\left.\frac{\partial U}{\partial x}\right|_{t}, \tag{3.14}$$

$$\left.\frac{\partial \ln A^2}{\partial \tau}\right|_{\xi} = -\frac{3}{2}\left.\frac{\partial U}{\partial x}\right|_{t} - \left.\frac{\partial C_g}{\partial x}\right|_{t}. \tag{3.15}$$

These equations can be integrated numerically along each characteristic with the initial conditions prescribed along any non-characteristic line. For example, since there is no internal-wave field for $t < 0$, the initial conditions for the surface waves can be selected along the $t = 0$ line. Thus,

$$x = x_0(\xi), \quad k = k_0, \quad A = A_0. \tag{3.16}$$

3.3. *Laboratory simulation*

The schematic of figure 5(*a*) is a mathematical idealization of the realistic condition that assumes that both the surface wave and the internal wave are monochromatically generated at $x = 0$. As shown in the x, t diagram, the surface wave is considered to be generated at all times, but the internal wave only exists for $t > 0$. Therefore, in the x, t diagram, a non-vanishing surface current exists only in the region bounded by the t axis and the internal-wave front $x = Ct$. Assuming that there is no variation of the internal-wave amplitude with x, the surface current field can be represented as

$$U = u_0 \sin K(x - Ct)\, H(x)\, H(t - x/C), \tag{3.17}$$

where $H(x)$ represents the Heaviside function such that

$$H(x) = \begin{cases} 1, & x > 0, \\ \tfrac{1}{2}, & x = 0, \\ 0, & x < 0. \end{cases}$$

The introduction of the Heaviside function is primarily for convenience in carrying out the analysis. However, because of the inherent slowly varying assumption implicit in the governing equations, this idealization must be justified, to ensure the correctness of the solution.

First, the real situation near the surface-wave maker must be analysed. Referring to figure 5(*b*), the magnitude of the surface current $|U|$ induced by the interfacial wave generated at $x = 0$ approaches the designed value u_0 at 'large' positive x. Because of the physical constraint of the surface-wave maker, the magnitude of the surface current at $x = 0$ must be near zero at the surface, but increases with depth to nearly the designed value in about one surface wavelength. Within the present depth-independent current assumption, an exact determination of the surface-current magnitude near $x = 0$ is difficult to make for the purpose of theoretical calculation. On the other hand, $|U|$ must vanish far to the left of the interfacial-wave generator. Therefore, a reasonably smooth surface-current field near the origin can be assumed as indicated in figure 5(*b*). For the purposes of demonstration, we assume

$$|U| = \tfrac{1}{2}u_0[1+\tanh(x/\Delta)]. \tag{3.18}$$

For $\Delta \gg \lambda_s$, the slowly varying assumption can be justified. On the other hand, for $\Delta \ll \lambda_i$, the solution to the problem of interest is relatively insensitive to the actual value of Δ when the absolute magnitude of u_0 is small. Numerical solutions of the equations using (3.18) with reasonable estimates for Δ have clearly demonstrated this insensitivity. Since (3.18) tends to the assumed surface-current field as Δ approaches zero, the use of a Heaviside function at $x = 0$ is justified in this sense. A similar argument can also be used near the internal-wave front $x = Ct$.

It should be noted that by using the Heaviside function as an approximation for the variation of the surface current the surface-wave conditions at $x = 0^+$ can be readily understood. Physically, the surface-wave maker is being driven by a motor at a given frequency and fixed stroke. When there is no surface current, the generated surface waves are characterized by k_0 and A_0. This situation changes when a surface current is present and the values of k and A at $x = 0^+$ are slightly different from k_0 and A_0 (which are presumed to exist for $x < 0$ in the present problem). The Heaviside function accounts for this slight jump in 'initial' conditions from $x = 0^-$ to $x = 0^+$.

With (3.17) or (3.18), (3.10), (3.14) and (3.15) can be integrated numerically to obtain solutions in the form of

$$k = k(x,t) \quad \text{and} \quad A^2 = A^2(x,t).$$

Instead, the first-order perturbation solutions of this set of equations are obtained in a closed form in § 3.4. With the solution given in an analytical form, features of the solution can be readily studied in great detail and the effects of the interaction phenomena can be displayed in a more explicit form.

3.4. *Perturbation solutions*

To simplify the analysis further, it is assumed that the magnitude of the surface current u_0 is small compared with the minimum of the group velocity for surface waves. For example, in the laboratory experiment u_0 is the order of $10^{-3}\,\mathrm{ft\,s^{-1}}$. Therefore, it is adequate to assume that

$$u_0/C_{g0} = \epsilon \ll 1,$$

where $C_{g0} = \frac{1}{2}(g/k_0)^{\frac{1}{2}}$, the unperturbed group velocity. Now, assume that the solutions can be represented by the following perturbation series in ϵ:

$$\begin{aligned} x &= x_0 + \epsilon x_1 + \epsilon^2 x_2 + \dots, \\ \ln k &= \ln k_0 + \epsilon \ln k_1 + \epsilon^2 \ln k_2 + \dots, \\ \ln A^2 &= \ln A_0^2 + \epsilon \ln A_1^2 + \epsilon^2 \ln A_2^2 + \dots, \\ C_g &= C_{g0} + \epsilon C_{g1} + \epsilon^2 C_{g2} + \dots, \end{aligned} \tag{3.19}$$

where $C_{g1} = -\frac{1}{2}C_{g0}.\ln k_1$.

Substituting (3.19) into (3.10), (3.14) and (3.15), and grouping terms of the same order in ϵ, one obtains for $O(\epsilon^0)$

$$\frac{\partial x_0}{\partial \tau} = C_{g0}, \quad \frac{\partial k_0}{\partial \tau} = 0, \quad \frac{\partial A_0^2}{\partial \tau} = -A_0^2 \frac{\partial C_{g0}}{\partial x} = 0. \tag{3.20}$$

These equations describe the unperturbed surface-wave field, which is assumed to be a uniformly generated monochromatic wave train. Therefore, integration of (3.20) gives

$$k_0 = \text{const.}, \quad A_0^2 = \text{const.}, \quad x_0 = C_{g0}(\tau - \xi), \tag{3.20a}$$

where ξ denotes the intersection of the characteristic with the t axis.

For $O(\epsilon)$ the governing equations become

$$\begin{aligned} \epsilon \frac{\partial \ln k_1}{\partial \tau} = -u_0[&K \cos K(x_0 - Ct)\, H(x_0)\, H(t - x_0/C) + \sin K(x_0 - Ct)\, \delta(x_0)\, H(t - x_0/C) \\ &- C^{-1} \sin K(x_0 - Ct)\, H(x_0)\, \delta(t - x_0/C)], \end{aligned} \tag{3.21}$$

$$\frac{\partial \ln A_1^2}{\partial \tau} = \frac{3}{2}\frac{\partial \ln k_1}{\partial \tau} - \frac{\partial C_{g1}}{\partial x}, \tag{3.22}$$

and

$$\epsilon \frac{\partial x_1}{\partial \tau} = u_0 \sin K(x_0 - Ct)\, H(x_0)\, H(t - x_0/C) + \epsilon C_{g1}, \tag{3.23}$$

where $\epsilon \ln k_1$ and $\epsilon \ln A_1^2$ represent the first-order change of the wavenumber and the square of the amplitude, while ϵx_1 gives the deviation from the unperturbed characteristic.

Using the zeroth-order characteristic, one obtains

$$x_0 - Ct = (C_{g0} - C)\,\tau - C_{g0}\xi. \tag{3.24}$$

Then the equations can be integrated from $\tau = 0$ to τ along a given characteristic $\xi = \text{const.}$ The solution to (3.21) should first be obtained, then used on the right-hand side of (3.22) and (3.23). Because of the appearance of the Heaviside functions the integration is lengthy, but it is straightforward. The solution for the wavenumber is given by

$$\begin{aligned} \epsilon \ln k_1 = \ln \frac{k}{k_0} = -\frac{u_0}{C_{g0} - C} H(x_0) \Big\{ &\sin K(x_0 - Ct)\, H(t - x_0/C) \\ &- \frac{C}{C_{g0}} \sin KC \left(\frac{x_0}{C_{g0}} - t\right) H(t - x_0/C_{g0}) \Big\}, \end{aligned} \tag{3.25}$$

and for the amplitude by

$$\ln\frac{A}{A_0} = -\frac{1}{4}\frac{u_0}{C_{g0}-C}H(x_0)\left\{\left(3+\frac{C_{g0}}{C_{g0}-C}\right)\sin K(x_0-Ct)\,H(t-x_0/C)-\frac{C}{C_{g0}}\right.$$
$$\left.\times\left[\left(4+\frac{C_{g0}}{C_{g0}-C}\right)\sin KC\left(\frac{x_0}{C_{g0}}-t\right)+\frac{C}{C_{g0}}Kx_0\cos KC\left(\frac{x_0}{C_{g0}}-t\right)\right]H\left(t-\frac{x_0}{C_{g0}}\right)\right\}. \quad (3.26)$$

For $k = k_0+\Delta k$, and $A = A_0+\Delta A$, the right-hand sides of (3.25) and (3.26) give the changes in wavenumber $(\Delta k/k_0)$, and wave amplitude $(\Delta A/A_0)$, respectively, for small changes. In practice, we are also interested in the change of the local surface-wave slope m, which is simply related to the changes in wavenumber and amplitude by

$$\ln\frac{m}{m_0} = \ln\frac{k}{k_0}+\ln\frac{A}{A_0}, \quad (3.27)$$

or for small variations by

$$\frac{\Delta m}{m_0} = \frac{\Delta A}{A_0}+\frac{\Delta k}{k_0}. \quad (3.27a)$$

It is also interesting to calculate the maximum changes in the surface-wavenumber, the amplitude and the slope at a given x station, as well as the corresponding phase of the internal-wave current where the maximum effect occurs. For the region where both Heaviside functions in (3.25) and (3.26) are equal to one, it is appropriate to drop the Heaviside function notation. Furthermore, define

$$\phi \equiv K(x_0-Ct) \quad \text{and} \quad \theta \equiv KC\left(\frac{x_0}{C_{g0}}-t\right) = \phi-B, \quad (3.28)$$

with

$$B \equiv Kx_0(1-C/C_{g0}).$$

Then (3.25), (3.26) and (3.27) can be rewritten as

$$\ln\frac{k}{k_0} = -\frac{u_0}{C_{g0}-C}\left[\sin\phi-\frac{C}{C_{g0}}\sin\theta\right],$$
$$\ln\frac{A}{A_0} = -\frac{1}{4}\frac{u_0}{C_{g0}-C}\left[\left(3+\frac{C_{g0}}{C_{g0}-C}\right)\sin\phi\right.$$
$$\left.-\frac{C}{C_{g0}}\left\{\left(4+\frac{C_{g0}}{C_{g0}-C}\right)\sin\theta+\frac{C}{C_{g0}}Kx_0\cos\theta\right\}\right], \quad (3.29)$$

and $$\ln\frac{m}{m_0} = -\frac{1}{4}\frac{u_0}{C_{g0}-C}\left[\left(7+\frac{C_{g0}}{C_{g0}-C}\right)\sin\phi\right.$$
$$\left.-\frac{C}{C_{g0}}\left\{\left(8+\frac{C_{g0}}{C_{g0}-C}\right)\sin\theta+\frac{C}{C_{g0}}Kx_0\cos\theta\right\}\right].$$

For a given x_0 and C/C_{g0}, the maximum or minimum change occurs at ϕ^*, the phase of the internal wave, where $\partial/\partial\phi(\quad) \equiv 0$. The quantity inside the parentheses can be any one of the three quantities given on the left of (3.29). The result of performing the indicated differentiations gives

$$\phi_k^* = \tan^{-1}\left(\frac{C_{g0}/C - \cos B}{\sin B}\right), \tag{3.30a}$$

$$\phi_A^* = \tan^{-1}\left\{\frac{3+\dfrac{C_{g0}}{C_{g0}-C}-\dfrac{C}{C_{g0}}\left[\left(4+\dfrac{C_{g0}}{C_{g0}-C}\right)\cos B+\dfrac{C}{C_{g0}}Kx_0\sin B\right]}{\dfrac{C}{C_{g0}}\left[\left(4+\dfrac{C_{g0}}{C_{g0}-C}\right)\sin B-\dfrac{C}{C_{g0}}Kx_0\cos B\right]}\right\}, \tag{3.30b}$$

and

$$\phi_m^* = \tan^{-1}\left\{\frac{7+\dfrac{C_{g0}}{C_{g0}-C}-\dfrac{C}{C_{g0}}\left[\left(8+\dfrac{C_{g0}}{C_{g0}-C}\right)\cos B+\dfrac{C}{C_{g0}}Kx_0\sin B\right]}{\dfrac{C}{C_{g0}}\left[\left(8+\dfrac{C_{g0}}{C_{g0}-C}\right)\sin B-\dfrac{C}{C_{g0}}Kx_0\cos B\right]}\right\}. \tag{3.30c}$$

The corresponding maximum or minimum values are obtained by substituting (3.30) into (3.29).

Since the solutions (3.25) and (3.26) appear to be inversely proportional to $C-C_{g0}$, a singular behaviour may seem to be probable at resonance. However, with a proper limiting procedure, it can be shown that, for $C_{g0} \to C$, we have

$$\ln\frac{k}{k_0} = -\frac{u_0}{C}H(x)\,H\left(t-\frac{x}{C}\right)[\sin K(x-Ct)+Kx\cos K(x-Ct)] \tag{3.31}$$

and

$$\ln\frac{A}{A_0} = -\frac{u_0}{4C}H(x)\,H\left(t-\frac{x}{C}\right)[(4-\tfrac{1}{2}K^2x^2)\sin K(x-Ct)+5Kx\cos K(x-Ct)], \tag{3.32}$$

where the subscript zero on x has been dropped, for convenience. Notice the strong dependence of the solutions on Kx, which effectively measures the distance or 'time' of interaction. Further, in the present model, the energy transfers only from the internal wave to the surface wave, and there is no provision to account for the limited energy available in the interval wave. Without considering the other nonlinear effects and the energy loss of the internal-wave train, the linearized solutions for the resonant case predict a monotonic increase of the effects with distance as shown by (3.31) and (3.32).

4. Results

The figures presented in §4 show results of the experiments as data points together with solid curves obtained from the present theory for the conditions of the experiments. The experimental and theoretical results both indicate that internal-wave-induced modulations of surface-wave amplitudes and slopes are largest when the internal-wave phase speed C and the group velocity of the undisturbed surface waves C_{g0} are equal (the 'resonant' condition). Figure 6 shows results from surface-wave slope modulation measurements as a function of x for a wave interaction configuration fixed near resonance ($C/C_{g0} \simeq 1$). A series of experiments of this type has been performed in which surface-wave amplitude

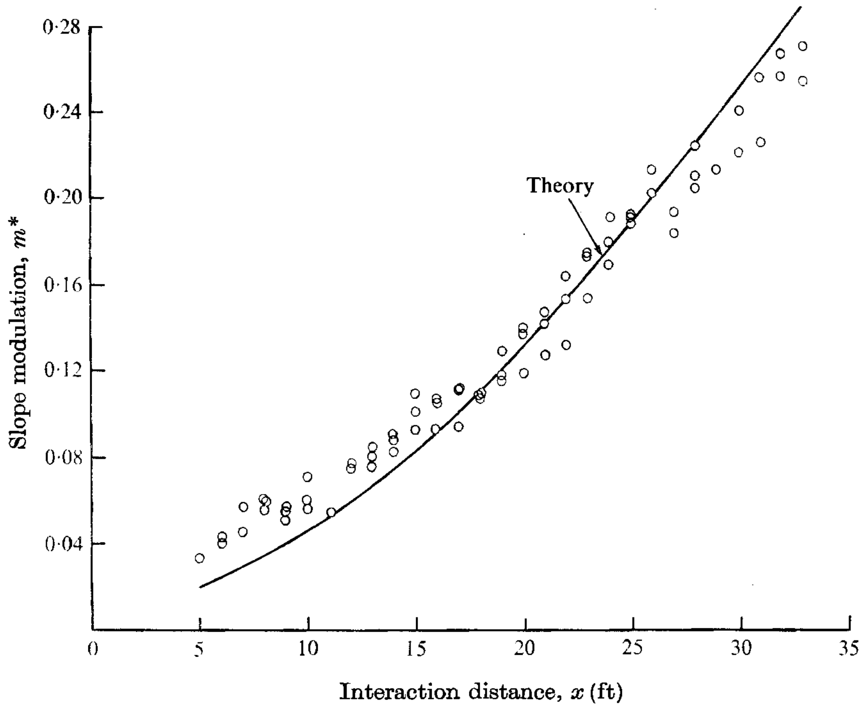

FIGURE 6. Surface-wave slope modulation against interaction distance $C/C_{g0} \simeq 1$. $\rho = 1{\cdot}152$, $T_i = 3{\cdot}9$ s, $k = 1{\cdot}92$ ft^{-1}, $c = 0{\cdot}84$ ft s^{-1}, $\bar{u}_0 = 6{\cdot}06 \times 10^{-4}$ ft s^{-1}.

and slope modulations have been measured as functions of the interaction distance x for configurations all of which are near resonance ($C/C_{g0} = 1{\cdot}00 \pm 2\,\%$). The interaction configurations are shown in table 1, and individual plots of the slope and amplitude modulations measured for each configuration are shown in Lewis & Lake (1973). The results shown in figure 6 are typical of the results of all such measurements, showing a good agreement with the present theory in magnitude and dependence on interaction distance for each configuration. The results of all amplitude and slope modulation measurements for these resonant interaction configurations are discussed further and presented in two composite plots in § 5.

The results of a second series of experiments demonstrate the dependence of internal-wave-induced surface-wave modulations on the relative wave speed C/C_{g0}. As described in § 2, these data were obtained by fixing the internal-wave conditions and the interaction distance and varying the surface-wave speed. Experiments of this type were performed for four different combinations of internal-wave conditions and interaction distances (as shown in table 1). Individual plots of the modulations measured for each combination of interaction conditions can be found in Lewis & Lake (1973). Figures 7 and 8 show sets of data from experiments of this type and are typical of the results obtained from all such experiments. All show good agreement with the present theory. In figure 7 the measured dependence of surface-wave slope modulations on relative wave speed is shown for two different interaction configurations. Comparison of the values of density ratio, internal wavenumber, internal-wave period and

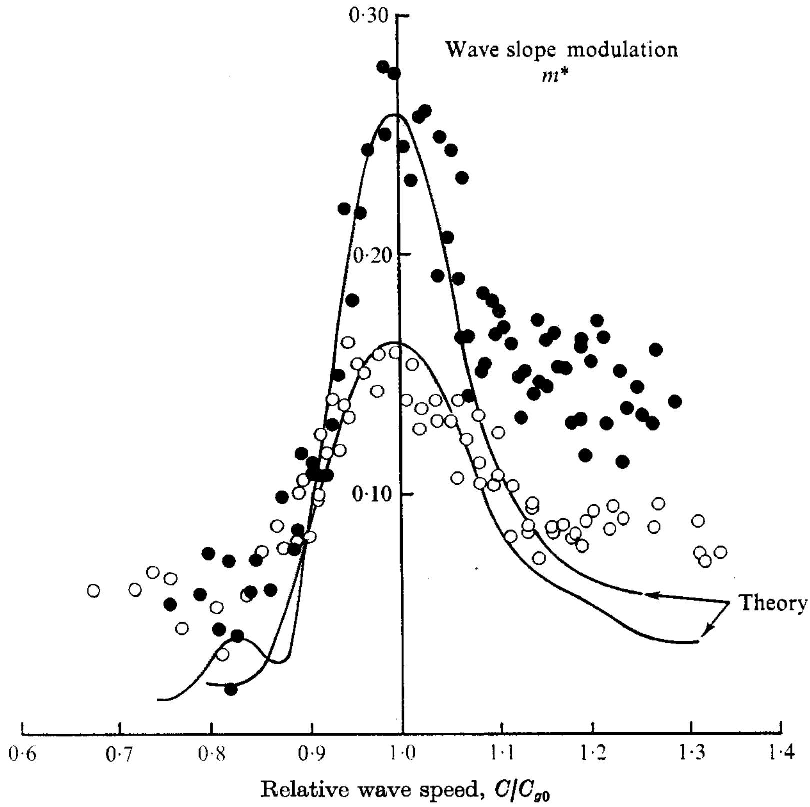

FIGURE 7. Surface-wave slope modulation against relative wave speed, equivalent interaction configurations at two values of Kx.

	ρ	T_i (s)	K (ft^{-1})	x (ft)	u_0 (ft s^{-1})	Kx
○	1·152	3·8	1·97	22·2	$5{\cdot}89 \times 10^{-4}$	43·8
●	1·152	3·9	1·93	30·0	$5{\cdot}54 \times 10^{-4}$	58·0

surface current for the two sets of results shows that all are closely matched, and therefore the modulation data in the two cases correspond to the same surface-wave/internal-wave interaction measured at two different interaction distances. In each case the results show that the maximum surface-wave slope modulations occur at 'resonance' where the wave speeds are matched, $C/C_{g0} = 1$. Comparison of the two sets of results shows further that, as the interaction distance increases, the magnitudes of the modulations at resonance increase (as found also in the resonant case measurements of figure 6), and the variation of modulation magnitudes with relative wave speed becomes increasingly 'narrow band' (i.e. the range of relative wave speeds for which modulation magnitudes are near the maximum or 'resonant' value decreases with increasing interaction distance). This effect is also predicted by the theory, which further predicts (Ko 1972) that, for relative wave speeds far from resonance, the dependence of the magnitude of the modulations on Kx is actually non-monotonic owing to destructive interference.

Figure 8 also shows results of surface-wave slope modulation measurements

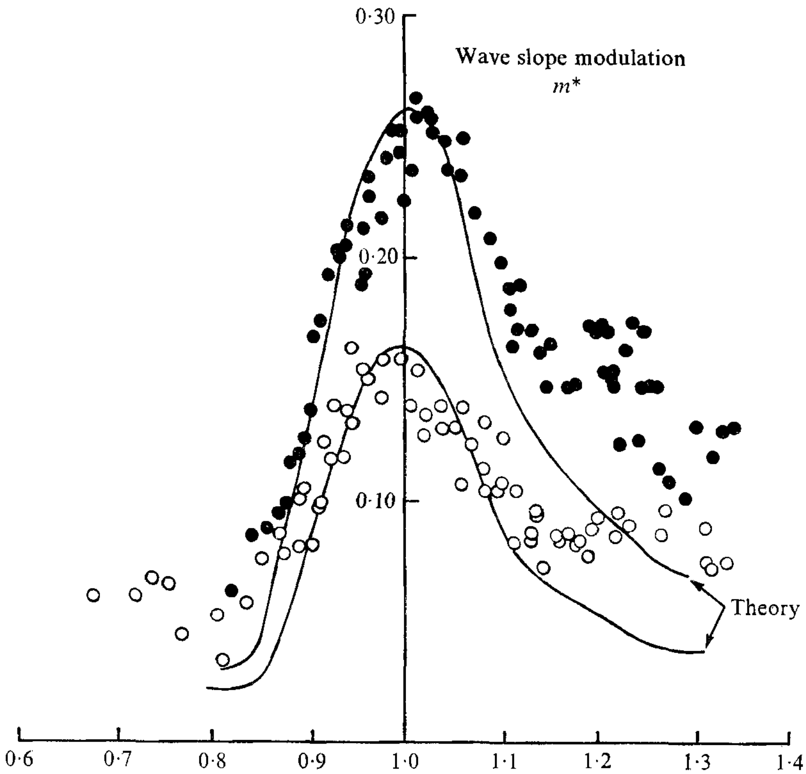

FIGURE 8. Surface-wave slope modulation against relative wave speed, two different interaction configurations with 'matched' values of Kx

	ρ	T_i (s)	K (ft^{-1})	x (ft)	u_0 (ft s^{-1})	Kx
○	1·152	3·8	1·97	22·2	$5\cdot89 \times 10^{-4}$	43·8
●	1·152	4·8	1·48	29·0	$1\cdot03 \times 10^{-3}$	42·8

for two different interaction configurations. In figure 8, however, the internal-wave conditions as well as the interaction distances are different for the two cases. Only the values of the interaction distance measured in internal wavelengths Kx are nearly equal in the two cases. Data from experiments of this type, in which modulations are measured against relative wave speed under different internal-wave conditions and different interaction distances, but with matched values of Kx, are used in § 5 to demonstrate that, by proper normalization, widely different modulation results can be reduced to a single form for slope and for amplitude.

The use of sensitive frequency-to-voltage converters has made possible the measurement of the small internal-wave-induced surface-wave frequency modulations, from which the surface wavenumber modulations can be obtained. The results of these measurements are shown in figure 9 for a series of experiments performed at fixed $Kx = 58$, in which measurements were made for a range of relative wave speeds. Although the wavenumber modulations were larger in this series of experiments than in any of the others, the actual magnitudes are still

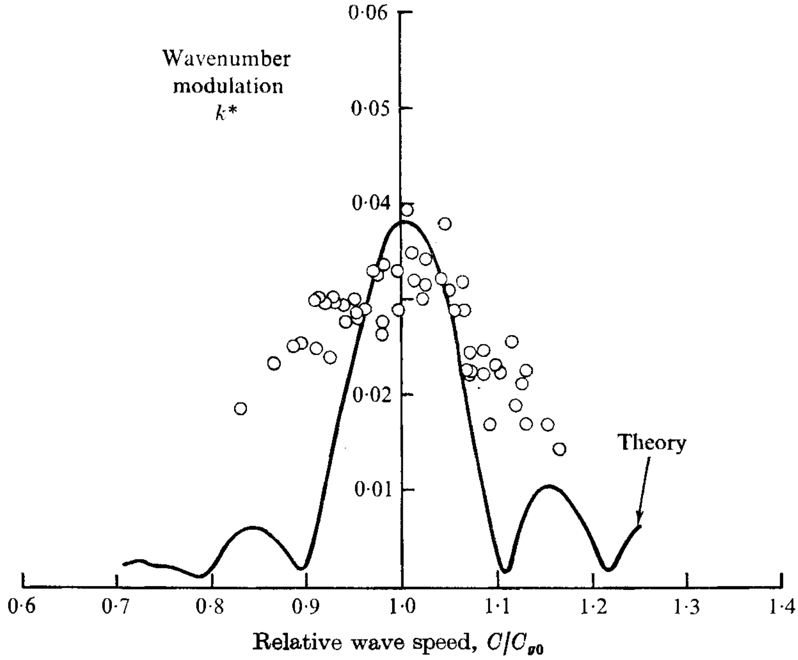

FIGURE 9. Surface-wavenumber modulation against relative wave speed for $Kx = 58$, $\rho = 1{\cdot}152$, $T_i = 3{\cdot}9$ s, $K = 1{\cdot}93\,\mathrm{ft}^{-1}$, $x = 30$ ft, $u_0 = 5{\cdot}54 \times 10^{-4}\,\mathrm{ft\,s}^{-1}$.

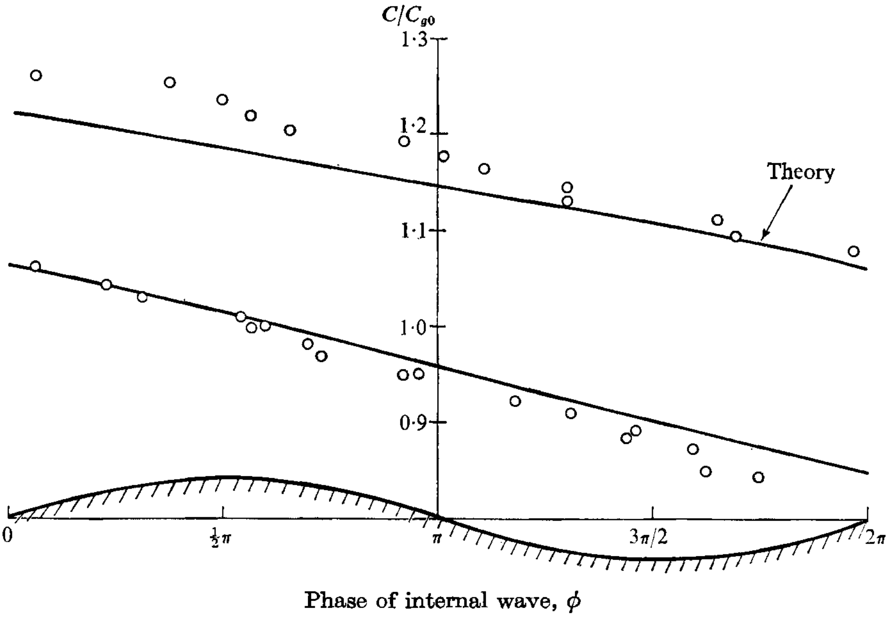

FIGURE 10. Phase location of maximum surface-wave slope modulation for $Kx = 42{\cdot}8$.

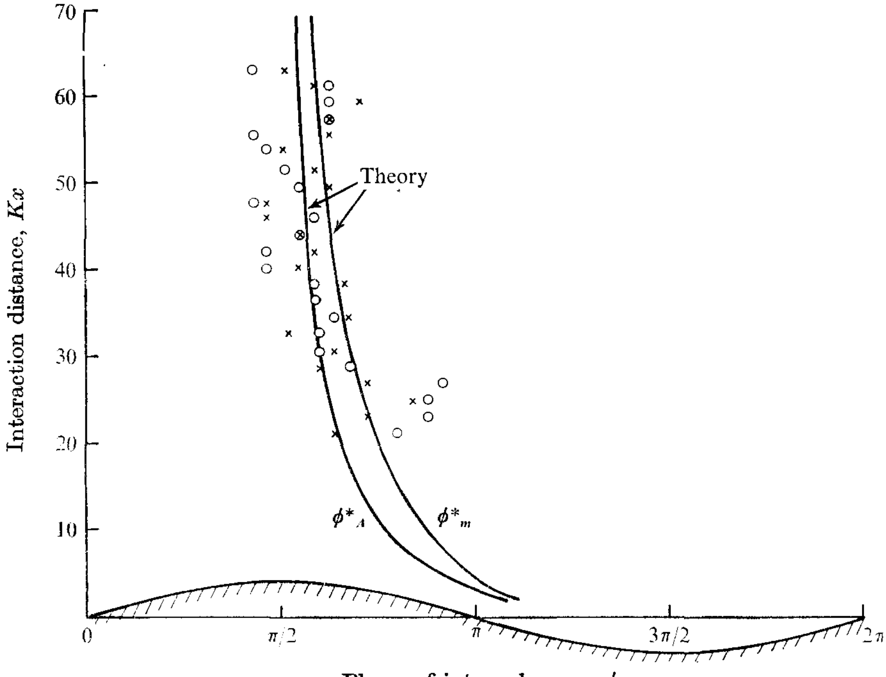

FIGURE 11. Effect of interaction 'distance' Kx on phase of internal wave where maximum slope and amplitude modulations occur for 'resonant' interactions. $C/C_{g0} \simeq 1$. $\bigcirc$, ϕ^* at $m^*_{\max}$; $\times$, ϕ^* at $A^*_{\max}$.

quite small, and accurate measurements are not possible over as wide a range of relative wave speed as is possible for slope or amplitude modulations. Nevertheless, the data are in good agreement in magnitude, and to some extent in variation with relative wave speed, with the predictions of the theory. The experimental confirmation of the small magnitude (4 % or less for these experiments, corresponding to $\Delta C_g/C_{g0} \leqslant 2$ %) of the wavenumber modulations, and therefore the group velocity modulations, produced by the wave interactions is of particular interest, since it is the latter condition on which the linearization in the analysis depends.

The phase of the internal wave at which maximum surface-wave modulation occurs has also been obtained from the experimental measurements. Figure 10 shows the internal-wave phase location of maximum surface-wave slope modulation for $Kx = 42{\cdot}8$. The data clearly show that the phase location of the maximum surface effect is a continuous and sensitive function of the relative speed of the internal and surface waves. Although the data have been obtained from oscillograph records and could be determined only to within approximately $\pm 10°$, the experimental and analytical results agree well in magnitude and rate of change of phase angle with relative wave speed in the range $0{\cdot}9 \lesssim C/C_g \lesssim 1{\cdot}1$, where the data are most reliable.

The measurements can also be used to describe the variation in the internal-wave phase location of maximum surface-wave slope and amplitude modulations with interaction distance Kx, for interactions at fixed relative wave speed. As shown in figure 11, the theory predicts that these phase locations asymptotically approach the internal-wave crest, $\phi = \frac{1}{2}\pi$, from values of $\phi > \frac{1}{2}\pi$ as Kx increases for resonant interactions. The experimental data for interaction conditions at or near resonance over a range of interaction distances from $Kx = 21$ to $Kx = 63$ are also shown in the figure. The data confirm that the phase location of maximum surface-wave slope and amplitude modulations approaches that of the interval-wave crest as Kx increases for resonant interactions.

5. Discussion

The experimental results demonstrate that for the 'resonant' case, surface-wave slope and amplitude modulations produced by internal-wave interactions with monochromatic surface waves increase monotonically with increased interaction distance. For fixed interaction distance, the variation in modulation magnitudes with relative wave speed is such that the maximum effect occurs at 'resonance', where the internal-wave phase speed and surface-wave group velocity are matched, and modulation magnitudes descrease rapidly as the relative wave speed diverges from the matched condition $C/C_{g0} = 1$. The decrease in modulation magnitudes as the relative wave speed diverges from $C/C_{g0} = 1$ is more rapid for $C/C_{g0} < 1$ (surface-wave groups outrunning internal waves) than for $C/C_{g0} > 1$ (internal waves outrunning surface-wave groups). As the interaction distance Kx increases, the variation of surface-wave modulation magnitudes with relative wave speed becomes increasingly 'narrow band', with maximum effects concentrated within a progressively narrower range of relative wave speeds centred around the 'resonant' condition. Surface-wave slope and amplitude modulations as large as 30 % have been measured and the experimental results are in good agreement with the theoretical predictions. At first, it may seem surprising that a 'linearized' theory can be valid with such large distortions. The explanation comes from the fact that the term 'linearization' is used in a somewhat different context for the present analysis. A simple observation of the system of equations displays the fact that the closed form solutions given by (3. 25) and (3.26) are a result of linearizing about the unperturbed characteristic slope C_{g0}. There is no further limitation on the changes in wave amplitude and slope provided that the dispersion relation (3.2) is still valid. This linearization about the characteristic slope implies that both u_0/C_{g0} and $\Delta C_g/C_{g0}$ are much less than one. Since $u_0/C_{g0} \sim O(0{\cdot}1\ \%)$, the main error in the linearization is introduced through the term $\Delta C_g/C_{g0}$. The maximum value of the term $\Delta C_g/C_{g0}$ (which is half of the change in wavenumber) over the experimental range of x stations satisfies $\Delta C_g/C_{g0} \lesssim 2\ \%$, which is well within the applicability of this linearization. The corresponding surface wavenumber modulations were measured and found to be $\leqslant 4\ \%$, also in agreement with the predictions of the theory. Measurements of the phase of the internal wave at which maximum surface-wave modulation occurs demonstrate that the phase location is a sensitive and continuous function of the relative wave speeds. For 'resonant' interactions, the internal-wave phase locations of the maximum surface-wave slope and amplitude modulations approach $\phi = \frac{1}{2}\pi$,

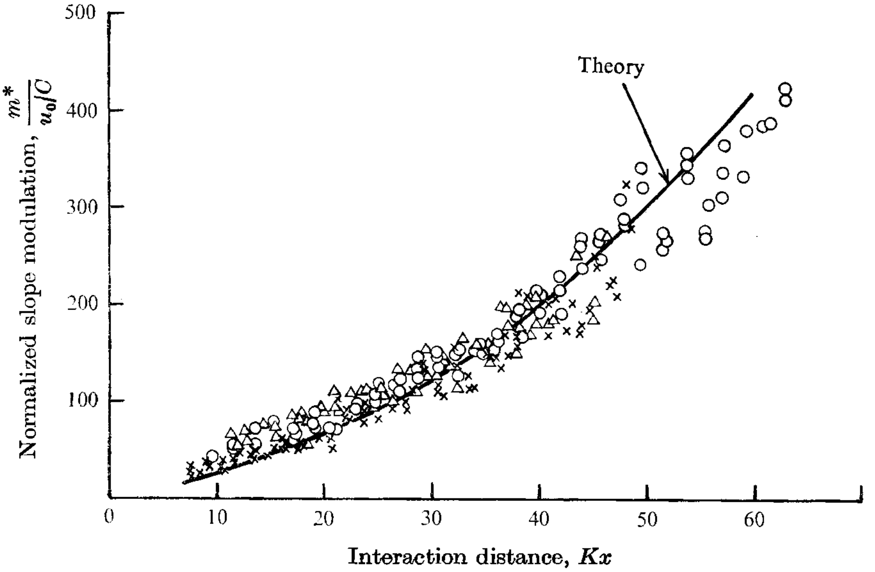

FIGURE 12. Normalized slope modulation against interaction 'distance' Kx. $C/C_{g0} \simeq 1$.

	ρ	T_i (s)
○	1·152	3·9
×	1·152	4·9
△	1·288	3·8

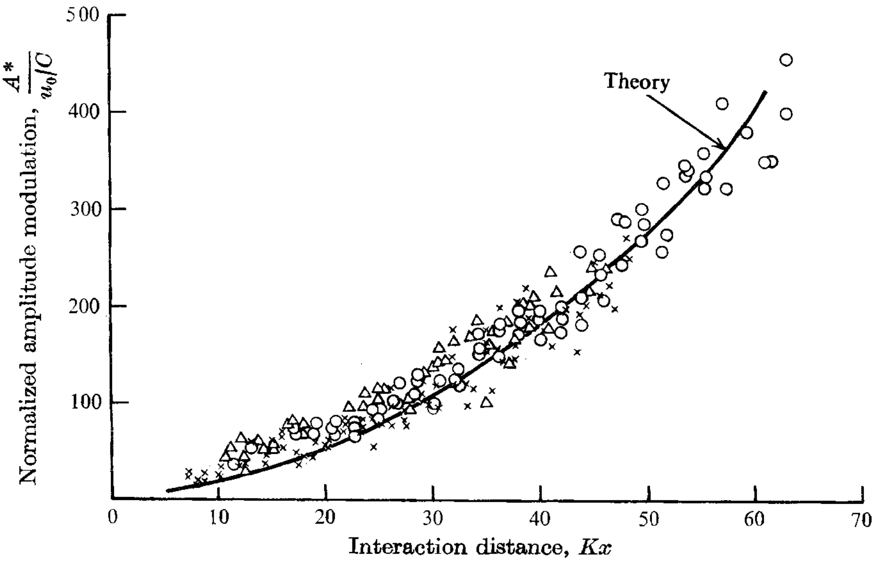

FIGURE 13. Normalized amplitude modulation against interaction 'distance' Kx. $C/C_{g0} \simeq 1$. Symbols as in figure 12.

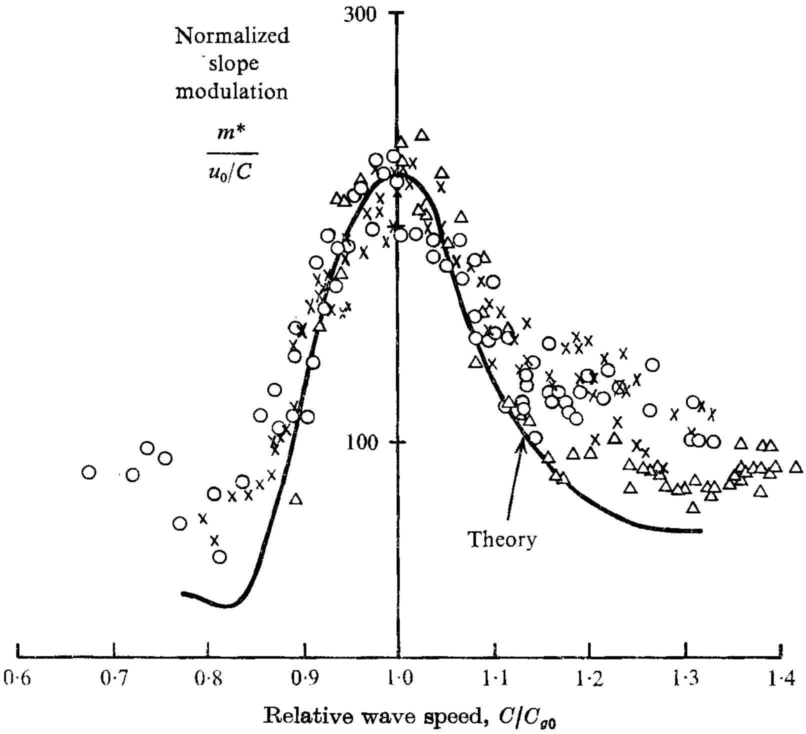

FIGURE 14. Normalized slope modulation against relative wave speed. $Kx \simeq 43$.

	ρ	T_i (s)
○	1·152	3·8
×	1·152	4·8
△	1·288	3·85

the location of the internal-wave crest, from locations at $\phi > \frac{1}{2}\pi$ as the interaction distance Kx increases.

Inspection of the analytical expressions for slope and amplitude modulations reveals that, when normalized by the ratio of induced surface current to internal-wave phase speed u_0/C, the 'resonant' case modulation magnitudes are dependent only on the interaction 'distance' Kx, and are independent of the magnitudes of the physical parameters in the problem, such as density ratio or internal-wave period or amplitude. Figures 12 and 13 show the results of applying this normalization to the experimental data. They include results from experiments at different density ratios and internal-wave periods, and therefore at different internal-wave decay rates, surface-current magnitudes, internal wavelengths and internal-wave phase speeds. Also shown in each figure is the normalized general result for resonant interactions obtained from the theory. The normalized experimental results describe single curves for normalized slope and amplitude modulations as functions of Kx, and agree with the normalized analytical results, confirming that the effects of the physical variables in the problem are properly accounted for when 'resonant' case wave interaction effects are expressed in this general form.

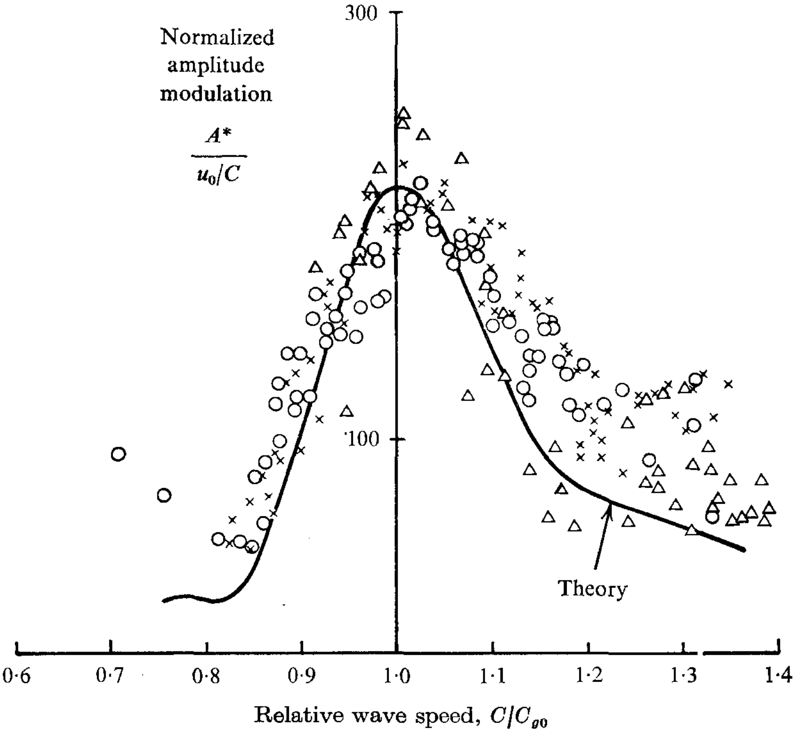

FIGURE 15. Normalized amplitude modulation against relative wave speed. $Kx \simeq 43$. Symbols as in figure 14.

The same normalization can be used to express the dependence of surface-wave modulations on relative wave speed in a general form independent of specific physical variables, as long as conditions are such that the interaction 'distance' Kx is fixed. This can be seen from figures 14 and 15, where experimental data from three very different interaction configurations are plotted in normalized form and compared with the normalized analytical results for slope and amplitude modulations versus relative wave speed at $Kx = 43$. The experimental data were from experiments performed under several different internal-wave conditions (density ratio, wave period, etc.) and interaction distances in combinations such that values of Kx were matched (actual values were 43·8, 42·8 and 42·9). For example, two of the sets of data in figure 14 are those shown before normalization in figure 8. Figures 14 and 15 show that, when the normalized modulation data are plotted against relative wave speed for these sets of matched Kx experiments, the data describe a single curve with experimental scatter no greater than in the individual sets alone, and the results agree well with the normalized analytical results. In this case, as in the 'resonant' case, evaluation of the experimental results using this more general normalized form demonstrates that the various experimental results are self-consistent, that the experimental and theoretical results are in good agreement, and that the influence of the physical variables on surface-wave modulations produced by internal-wave interactions with monochromatic surface waves has been correctly identified.

6. Conclusions

Experiments were performed in which the effects of one-dimensional internal-wave interactions with linear monochromatic surface gravity waves were measured. The interactions produce surface-wave amplitude and slope modulations that are sinusoidal and have the frequency of the internal wave. The magnitude of the modulations depends strongly on the relative wave speeds, and is a maximum when the phase speed of the internal wave C and the group velocity of the surface wave C_{g0} are matched (the 'resonant' condition). The magnitude increases monotonically with increased internal-wave induced surface current, and, for conditions at or near resonance, with increased interaction 'distance' or interaction 'time' as measured by Kx. As Kx increases, the variation of surface-wave modulation magnitudes with relative wave speed becomes concentrated within a progressively narrower range of relative wave speeds centred around the resonant condition. Surface-wave amplitude and slope changes of more than 30 % were measured in the experiments. For the same conditions, measured surface wavenumber changes were less than 4 %, corresponding to changes in surface-wave group velocity of less than 2 %. The phase of the internal wave at which maximum surface-wave modulation occurs was measured, and was found to be a sensitive and continuous function of the relative wave speeds.

A closed form linearized solution to the wave and energy conservation equations was obtained. The experimental results are in good agreement with the present theory. Normalization of slope and amplitude modulation data reduced results of measurements made under differing interaction conditions (for which either $C/C_{g0} = 1$ or $Kx = \text{const.}$ was maintained) to more general forms, further demonstrating the agreement between experiment and theory.

The authors gratefully acknowledge the contributions of Harald Rungaldier and Dewey J. Rowland, who provided invaluable assistance in the construction and carrying out of the experiments. This study was supported by the Applied Physics Laboratory of Johns Hopkins University under contract APL/JHU 341768.

REFERENCES

Ewing, G. 1950 *J. Mar. Res.* **9**, 161.

Gargett, A. E. & Hughes, B. A. 1972 On the interaction of surface and internal waves. *J. Fluid Mech.* **52**, 179.

Hartle, J. B. & Zachariasen, F. 1968 The interaction of internal waves and gravity waves. *JASON* 1968 *Summer Study, Inst. of Defense Analysis Study*, S-334.

Ko, D. R. S. 1972 A conservational approach to the interaction of internal waves and surface waves. *TRW Rep.* 18202-6001-R0-00, vol. 4; APL/JHU issuing no. POR-3534.

LaFond, E. C. 1962 *The Sea* (ed. N. M. Hill), vol. 1, pp. 731–751.

Lewis, J. E. & Lake, B. M. 1973 Experimental investigations of the interaction of internal waves and surface gravity waves. *TRW Rep.* 18202-6010-RU-00; APL/JHU issuing no. POR-3569.

Longuet-Higgins, M. S. & Stewart, R. W. 1960 Changes in the form of short gravity waves on long waves and tidal currents. *J. Fluid Mech.* **8**, 565.

LONGUET-HIGGINS, M. S. & STEWART, R. W. 1961 The change in amplitude of short gravity waves on steady non-uniform currents. *J. Fluid Mech.* **10**, 529.

NEUMANN, G. & PIERSON, W. J. 1966 *Principles of Physical Oceanography*, p. 294. Prentice-Hall.

PHILLIPS, O. M. 1969 *The Dynamics of the Upper Ocean*. Cambridge University Press.

PHILLIPS, O. M. 1971 Surface wave effects produced by internal waves. *Hydronautics TR*, no. 7015-3.

WHITHAM, G. B. 1962 Mass, momentum and energy flux in water waves. *J. Fluid Mech.* **12**, 135.

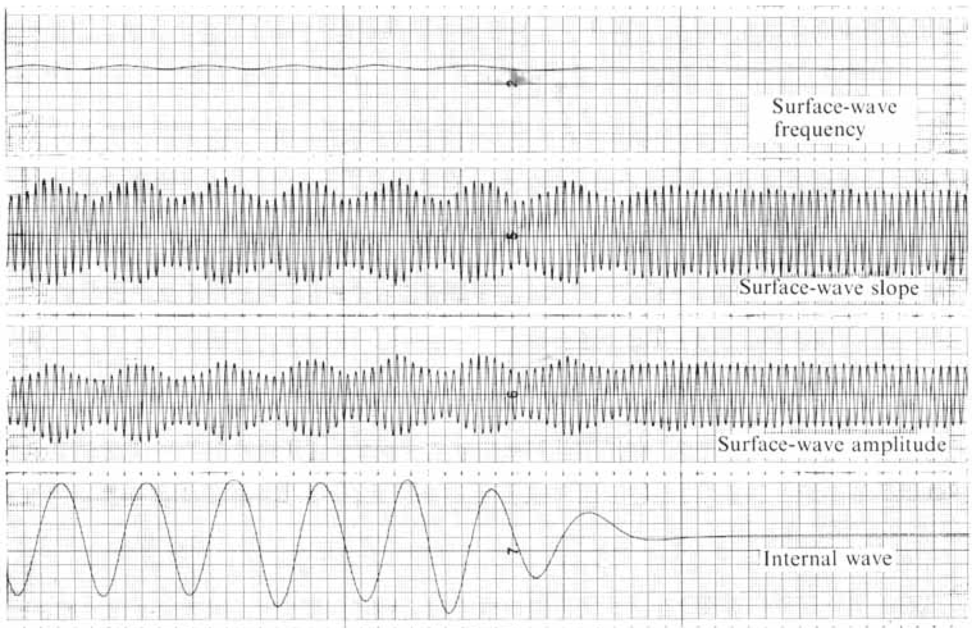

FIGURE 4. Oscillograph records, showing onset of interaction of internal wave with surface wave.